Effects of finite non-Gaussianity on evolution of a random wind wave field

S. Y. Annenkov [1,2] and V. I. Shrira [1]

[1]*School of Computing and Mathematics, Keele University, Keele ST5 5BG, United Kingdom*
[2]*Shirshov Institute of Oceanology, Russian Academy of Sciences, Moscow 117997, Russia*

We examine the long-term evolution of a random wind wave field generated by constant forcing, by comparing numerical simulations of the kinetic equation and direct numerical simulations (DNS) of the dynamical equations. While the integral characteristics of the spectra are in reasonably good agreement, the spectral shapes differ considerably at large times, the DNS spectral shape being in much better agreement with field observations. Varying the number of resonant and approximately resonant wave interactions in the DNS numerical scheme, we show that when the ratio of nonlinear and linear parts of the Hamiltonian tends to zero, the DNS spectral shape approaches the shape predicted by the kinetic equation. We attribute the discrepancies between the kinetic equation modeling, on one side, and the DNS and observations, on the other, to the neglect of non-Gaussianity in the derivation of the kinetic equation.

Introduction. The long-term nonlinear evolution of random wave fields is described by wave turbulence theory, which links ensemble averaged quantities of the field to the spectral density $n_{\mathbf{k}} = n(\mathbf{k}, t)$, a function of wave vector $\mathbf{k}$ and time t [1]. This quantity, proportionate to the Fourier transform of two-point averages, is called the particle number, power, or wave-action density in various contexts. Often, there is an inverse cascade of this quantity towards large scales, leading to the emergence of long waves due to resonant interactions of shorter waves. Within the wave turbulence theory, the process is described by the kinetic equation (KE), which expresses time derivatives of the density in terms of this density only [1,2]. Analytical and numerical solutions of this equation form the core of our understanding of the evolution of random wave field on large timescales.

By far the most studied example of this evolution is provided by oceanic wind waves. The corresponding KE is known as the Hasselmann equation [3], and is routinely simulated numerically for operational wave forecasting. From the theoretical perspective, the wind wave example stands out due to continuous worldwide testing of the forecasting against observations, which gives a unique chance to verify the assumptions underlying the wave turbulence theory.

While there is a consensus that the KE does capture the main features of wave field evolution [4–8], there are major discrepancies between the KE-based predictions and observations. The inherent property of the KE is the homogeneity of the wave interaction term as a function of spectral energy density [8]. This property leads to self-similarity of the solutions in a wide range of wave generation conditions [9] and allows us to formulate the basic laws of wind wave growth independently of wind speed [8]. In an idealized situation when a wave field is generated by constant wind, the KE predicts that the solution tends to a permanent self-similar shape, with a characteristic enhanced peak and steep, nearly straight

spectral front, which evolves towards large scales following the known asymptotic laws (e.g., Ref. [9]). As long as the consideration is confined to the integral characteristics of a wave field (such as a significant wave height, total energy, frequency of the spectral peak), the self-similar picture of wind wave development predicted by the KE is generally supported experimentally [5,6,8]. However, a closer look at spectral shapes reveals a major discrepancy: The observed spectral shapes of young and mature sea states essentially differ [Joint North Sea Wave Project (JONSWAP) and Pierson-Moskowitz spectra, respectively] [10]. As waves mature, a decrease in the spectral peakedness is observed [7,11–13]. The parametrization of the spectral shape of a fully developed sea, proposed in Ref. [14], confirmed in a later reanalysis [15], and at present widely accepted to be well assured statistically [11], is different from the shape of the self-similar KE solutions, having a more rounded spectral front and peak with no pronounced enhancement. The evolution of the spectral shape with fetch with a decrease of peakedness and a continuous transition to the Pierson-Moskowitz spectrum has been described in a number of measurement-based studies [7,11–13]. At this stage of wave field development, the spectral peak is no longer under direct wind forcing, and the probability of breaking events for dominant waves is low [15,16], so that the shape of the peak should be determined primarily by nonlinear interactions. Therefore, the fact that the KE is unable to reproduce this spectral shape represents a major fundamental challenge.

Until recently, the KE as the model of long-term wind wave field evolution did not have an alternative (a generalization proposed by Ref. [17], although useful, in the large time limit tends to the KE and, hence, does not resolve the contradiction). This situation was changed when a direct numerical simulation (DNS) algorithm capable of long-term simulations of random wave fields was proposed [18–20]. The algorithm is based on the Zakharov equation, from which the KE is

derived, and performs simulations with ensemble averaging without any statistical assumptions. DNS simulations without wind showed, in particular, that in contrast to the KE predictions, the DNS spectra have a less steep, more rounded spectral front and a considerably wider and lower peak [20]. At the same time, no apparent reason to question the basic assumptions underlying the wave turbulence theory (e.g., smallness of non-Gaussianity, wide separation of timescales) has been found, and an explanation of the discrepancies remained outstanding.

In this Letter, we identify the origin of the discrepancies as the neglect of small but finite non-Gaussianity in the derivation of the KE itself, rather than in the underlying theory. In order to get a closed equation in terms of $n_{\mathbf{k}}$, one has to express the six-point correlator in terms of two-point ones only, neglecting the four-point cumulants in the expansion [21]. This approximation, equivalent to the assumption of random initial phases [22], leads to the aforementioned homogeneity property, absent in the primitive equations, and contradicts the established picture of weak turbulence, according to which the wave field evolution is due to the nonlinear regeneration of non-Gaussianity [23]. Thus, the KE takes into account finite nonlinearity (the asymptotic expansion in powers of nonlinearity retains cubic terms), but assumes infinitesimal non-Gaussianity. Crucially, according to the KE the spectral shape is the same for all levels of nonlinearity, including infinitesimal nonlinearity. In this sense, the neglect of finite non-Gaussianity does not allow one to properly capture the effects of finite nonlinearity either.

To consider the effects of finite non-Gaussianity on the long-term evolution of a random wave field, we examine by DNS the evolution of a wave field generated by constant wind, and compare it with the KE results. In both models,

the evolution tends to self-similarity, and the integral characteristics of the spectra are close to each other. However, the shape of the DNS spectra is quite different, with a lower, less pronounced peak. Introducing integral characteristics of the non-Gaussianity linked to the coarse-graining parameter of the numerical scheme, we find the wave spectrum dependence on non-Gaussianity, and demonstrate that the DNS spectral shape converges to the KE one when the non-Gaussianity tends to zero. This enables us to attribute the origin of the discrepancy to the neglect of non-Gaussianity in the KE derivation.

Theoretical background and numerical methods. We consider gravity waves on the surface of deep fluid governed by the Zakharov equation [1]

$$i\frac{\partial b_0}{\partial t} = \omega_0 b_0 + \int T_{0123} b_1^* b_2 b_3 \delta_{0+1-2-3} \, d\mathbf{k}_{123}. \quad (1)$$

Here, $b(\mathbf{k})$ is a canonical complex variable in Fourier space, $\mathbf{k}$ is the wave vector, $k = |\mathbf{k}|$, and $\omega(\mathbf{k}) = (gk)^{1/2}$ is the linear dispersion relation. The compact notation used designates arguments by indices, e.g., $T_{0123} = T(\mathbf{k}, \mathbf{k}_1, \mathbf{k}_2, \mathbf{k}_3)$, $\delta_{0+1-2-3} = \delta(\mathbf{k} + \mathbf{k}_1 - \mathbf{k}_2 - \mathbf{k}_3)$, an asterisk means complex conjugation, and t is time.

For wave fields with the $2 \leftrightarrow 2$-type dominant resonant process (1) is often taken as the primitive equation (thus, higher-order resonances are neglected). Then the statistical description of a wave field can be obtained in terms of correlators of $b(\mathbf{k}, t)$ as [17]

$$\frac{\partial n_0}{\partial t} = 2 \, \text{Im} \int T_{0123} J_{0123}^{(1)} \delta_{0+1-2-3} \, d\mathbf{k}_{123}. \quad (2)$$

where n_0 is the second-order correlator, $\langle b_0^* b_1 \rangle = n_0 \delta_{0-1}$, and $J_{0123}^{(1)}$ is the four-point cumulant. In the next order [21],

$$\left(\frac{\partial}{\partial t} - i\Delta\omega\right) J_{0123}^{(1)} = 2i \int \{T_{0456}\delta_{0+4-5-6}I_{156234} + T_{1456}\delta_{1+4-5-6}I_{056234} - T_{2456}\delta_{2+4-5-6}I_{014356} - T_{3456}\delta_{3+4-5-6}I_{014256}\}d\mathbf{k}_{456},$$

$$(3)$$

where $\Delta\omega = \omega_0 + \omega_1 - \omega_2 - \omega_3$, and I_{012345} is the six-point correlator. Since the six-point cumulant is neglected, I_{012345} is reduced to a lengthy expression containing pair correlators and four-point cumulants. Thus, the system of equations for two- and four-point correlators is closed. However, to obtain the closed equation for $n_{\mathbf{k}}$, we must neglect all four-point cumulants in the expansion for I_{012345}, retaining only the leading-order term. Such a reduction is equivalent to the Gaussianity assumption. The resulting KE is

$$\frac{\partial n_0}{\partial t} = 4\pi \int T_{0123}^2 f_{0123} \delta_{0+1-2-3} \delta(\Delta\omega) d\mathbf{k}_{123}, \quad (4)$$

where $f_{0123} = n_2 n_3 (n_0 + n_1) - n_0 n_1 (n_2 + n_3)$. Equivalently, the KE can be derived by assuming initial random phases [22].

The neglect of weak non-Gaussianity in the derivation of the KE makes its right-hand side a homogeneous function of $n(\mathbf{k})$ [8]. This means that the shape of the solutions for spectra provided by the KE corresponds to the case of infinitesimal amplitude. Thus the role of finite amplitude effects remains unknown. In an attempt to study these effects, we compare

numerical simulations based on the KE and the Zakharov equation (1). The Zakharov equation is simulated using the original algorithm, described in Ref. [20]. All parameters of the algorithm are the same as in Ref. [20], except for three modifications. First, in contrast to the simulations of swell in Ref. [20], we add wind forcing according to Ref. [24], for all $k < 4.84$. Second, to accommodate the wider angular distribution of the wind wave spectra, we increase the range of angles, retaining the same angular resolution. Thus, the computational grid contains 161 logarithmically spaced wave numbers in the range $0.25 \leqslant k \leqslant 9$ and 71 angles in the range $-7\pi/9 \leqslant \theta \leqslant 7\pi/9$. Third, a DNS algorithm with wind forcing can only be functional if a certain parametrization of wave breaking is employed. Here, we do not attempt to model the physical process of wave breaking, but intermittency in individual realizations makes it necessary to limit the growth of some wind amplified harmonics. To this end the following empirical rule is introduced: If the nondimensional value $\varepsilon_k = 0.5\sqrt{2\omega n_{\mathbf{k}}/g}/\pi k$ exceeds ε_c, where $n_{\mathbf{k}}$ is the discrete wave action of a harmonic under forcing, then the forcing
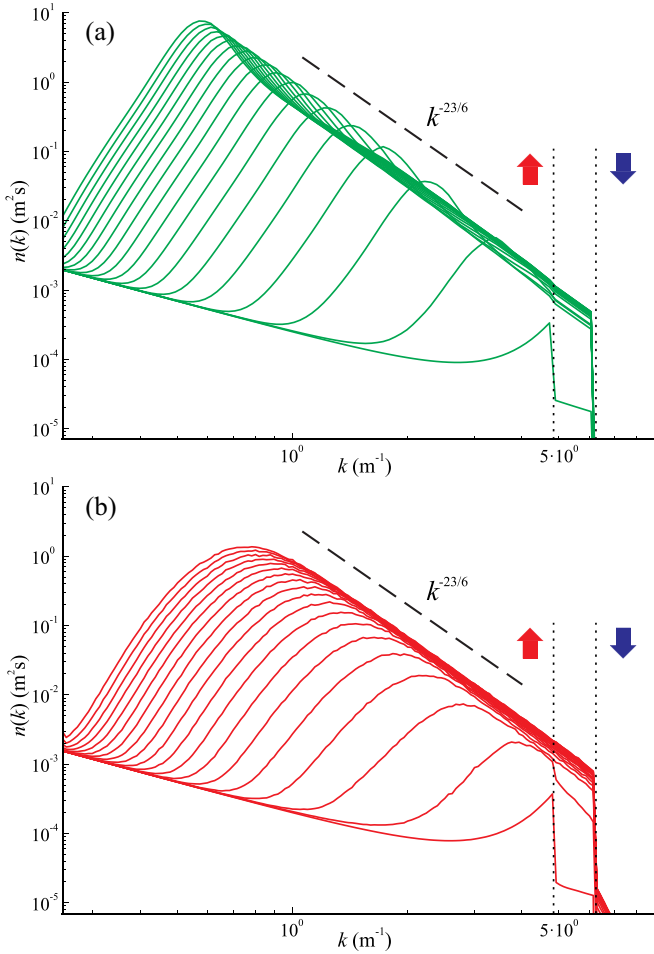
FIG. 1. Development of wave action spectrum $n(k)$ under constant wind $U = 2c_1$, shown in steps of approximately $300\tau_1$, where c_1 and τ_1 are the characteristic phase speed and period, corresponding to $k = 1$. (a) KE, WRT algorithm, and (b) DNS, with $\lambda_k = 0.03$ on a 161×71 grid. Wave-number ranges of forcing and dissipation are indicated by arrows.

is changed to damping until $\varepsilon_k \leqslant 0.1\varepsilon_c$, when it is resumed. For the simulations with the 161×71 grid, ε_c is set to 0.01, resulting in a small number of "breaking events," usually between 0 and 5 for each realization at every time step. A detailed discussion of the structure of the DNS algorithm and the role of parameters λ_k and ε_c, with a number of additional simulations, is provided in the Supplemental Material [25].

For the KE simulations, we use the standard Webb-Resio-Tracy (WRT) algorithm, provided by van Vledder, and a 101×51 grid with the same range of wave numbers and a full circle of directions. Wind forcing is identical for both models, and dissipation is applied to $k \geqslant 6.25$.

Results. First, we perform simulations of the wave field development from zero initial condition under forcing by constant wind with speed $U = 2c_1$, where c_1 is the phase speed corresponding to $k = 1$, close to the peak wave number at the end of the evolution. The DNS simulation is performed with averaging over 100 realizations. Development of the wave action spectrum $n(k)$ with time for both numerical methods is shown in Fig. 1. A comparison of the panels shows

that both solutions tend to self-similar behavior, and that the asymptotics of duration-limited wave growth under constant wave action flux, known from the analysis of the KE [9], are respected in both cases. However, the spectral shapes, which are initially close, differ considerably at later stages of the evolution. Although the spectral slope in both cases corresponds to the theoretical value for the inverse cascade of wave action $k^{-23/6}$ [21], the DNS spectra have a less steep, more rounded spectral front and a considerably wider and lower peak. Similar differences were reported earlier for simulations of wave evolution without wind forcing [20]. In the present case, the KE evolution also demonstrates a slightly faster downshift rate.

Due to the homogeneity property of the KE, the self-similar spectral shape is the same for all levels of nonlinearity, and the downshift rate has a simple scaling law [8]. If the discrepancies between the KE and the DNS are due to the effects of non-Gaussianity unaccounted for by the KE, they are expected to decrease at lower levels of nonlinearity. Simulations with lower wind forcing indeed show that the difference in the downshift rate decreases, but the difference in spectral shapes persists. Our aim to compare the DNS and the KE evolution in the small nonlinearity limit cannot be done by simply decreasing the wind speed, since wind-generated waves always have a certain finite steepness.

Here, we use another approach, which is helped by the particular design of the DNS algorithm. The algorithm is based on the idea of coarse graining of a wave field [20], which relaxes the resonance condition into $\mathbf{k}_0 + \mathbf{k}_1 - \mathbf{k}_2 - \mathbf{k}_3 = \Delta \mathbf{k}$. In contrast to the standard condition $\Delta \mathbf{k} = 0$, the wave vector and frequency mismatches satisfy $\Delta\omega/\omega_{\min} < \lambda_\omega$, $|\Delta\mathbf{k}|/k_{\min} < \lambda_k \bar{\omega}/\omega_{\min}$, where $\omega_{\min}$ and $k_{\min}$ are the minimum values of frequency and wave number in the quartet, $\bar{\omega}$ is the mean frequency, and λ_ω and λ_k are the detuning parameters. A crucial role is played by the coarse-graining parameter λ_k. If $\lambda_k = 0$, the wave field in the canonically transformed space, in which both the Zakharov equation and the KE operate, is free (Gaussian) regardless of the amplitude, since a logarithmically spaced grid with $\lambda_k = 0$ allows no nontrivial wave interactions and, hence, no evolution. When λ_k is increased, the number of approximately resonant interactions (with fixed $\lambda_\omega = 0.01$) grows approximately quadratically with λ_k, while the rate of spectral evolution, measured by the rate of change of various integral parameters, quickly increases, until it reaches saturation at a certain value λ_k, dependent on the grid resolution. Since in Ref. [20] the value $\lambda_k = 0.03$ was found to be optimal for the 161×71 grid, this value was used while computing the DNS evolution shown in Fig. 1. For the purpose of this study, it is convenient to use λ_k as a way to create wave fields with the same level of nonlinearity ε, but different levels of non-Gaussianity. In order to avoid discreteness artifacts at a low number of interactions, we use, along with the 161×71 grid, the refined 321×71 grid, setting $\varepsilon_c = 0.0075$ and λ_k in the range $0.003 \leqslant \lambda_k \leqslant 0.03$. Non-Gaussianity can be measured as the ratio of the nonlinear part of the ensemble averaged Hamiltonian $\bar{H}$ [19],

$$\bar{H}_{\mathrm{NL}} = \frac{1}{2} \int T_{0123} \langle b_0^* b_1^* b_2 b_3 \rangle \delta_{0+1-2-3} \, d\mathbf{k}_{0123}, \qquad (5)$$

and its linear part $\bar{H}_L = \int \omega_0 n_0 \, d\mathbf{k}_0$.
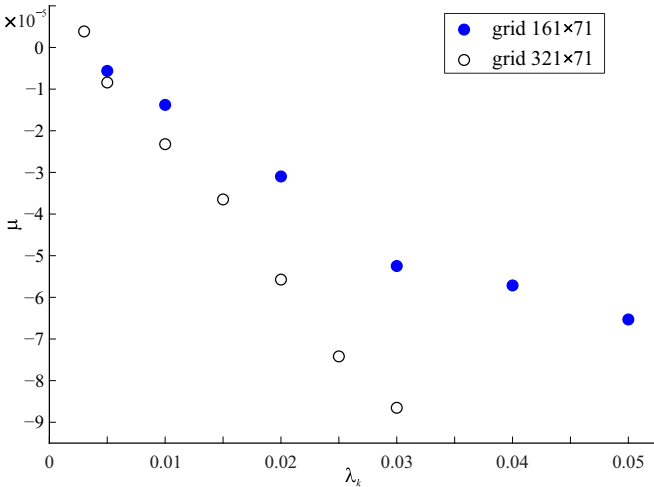
FIG. 2. Non-Gaussianity as measured by μ, the ratio of statistically averaged nonlinear and linear energy as a function of the coarse-graining parameter λ_k. μ is averaged over 600 characteristic periods of the final stage of evolution before the spectral peak reaches $k_p = 1$.

FIG. 3. Self-similar shape function $\mathcal{U}(\xi)$, $\xi = kt^{6/11}$, extracted from the numerical solutions at the last 1000 wave periods of evolution. Shapes at every 100 periods are shown in light colors, and the final curve is in a darker color of the same hue, normalized for $\mathcal{U}(1) = 1$. Numerical models used are the KE and the DNS on 161×71 (DNS161) and 321×71 (DNS321) grids for different values of λ_k.

The evolution of all wave fields is traced by the DNS with the same wind forcing as above, until the peak of the wave action spectrum $n(k)$ reaches $k_p = 1$. Under the wind forcing, the linear and nonlinear parts of the Hamiltonian both grow with time, but their ratio $\mu = \bar{H}_{\mathrm{NL}}/\bar{H}_L$ is approximately constant at the self-similar stage of evolution. The nonzero value of μ, although very small, is a prerequisite for spectral evolution. Figure 2 shows the value of μ averaged over the last 600 periods of evolution before reaching $k_p = 1$ for both grids, as a function of λ_k. Non-Gaussianity quickly grows with an increase of λ_k, approaching saturation at $\lambda_k \geqslant 0.03$. Meanwhile, the spectral evolution, as described by various integral parameters, does converge for both grids, and is very close between them. Formally, the value of λ_k required for the simulation can be made smaller by a further refinement of the grid, although in practice this is limited by the available computational resources. In particular, on the refined 321×71 grid the number of wave interactions exceeds 10^9 already for $\lambda_k = 0.01$.

We are mainly interested in the shape of the spectrum. At the self-similar stage of evolution the spectral shape is characterized by the self-similar function $\mathcal{U}$ for the duration-limited evolution, $n(k) = at^{23/11}\mathcal{U}(bkt^{6/11})$, where a and b are constants [9]. The simulated self-similar spectral shapes $\mathcal{U}(\xi)$ are shown in Fig. 3. While the spectral slope depends on the parametrization of breaking more than on λ_k, the shape of the spectral front demonstrates a clear dependence on λ_k. For small λ_k, the wave field has relatively few wave interactions (about 10^8 on the 321×71 grid at $\lambda_k = 0.003$), and the evolution is very slow, although the self-similar state is eventually reached, with the spectral front of the shape function $\mathcal{U}(\xi)$ close to the KE shape function. With the increase of λ_k from zero, the shape function quickly approaches a different form, with a more rounded front and a wider peak, resembling the Pierson-Moskowitz spectral shape.

For many applications, the evolution and prediction of the integral characteristics of the spectra, such as significant wave height, is of particular importance [4]. The key question is whether the evolution of integral characteristics can be affected by the effects of finite non-Gaussianity for realistic wind speeds. To clarify this point, we plot in Fig. 4 the evolution of significant wave height H_s obtained with the KE and the DNS for various values of λ_k. Figure 4 demonstrates that with an increase of λ_k the DNS evolution of H_s converges, remaining slightly slower than that predicted by the KE, but following the same asymptotic rate of increase known for the KE in the case of constant action flux [9]. The difference between the KE and the DNS is mostly manifested in the spectral shape, while the difference in significant wave height
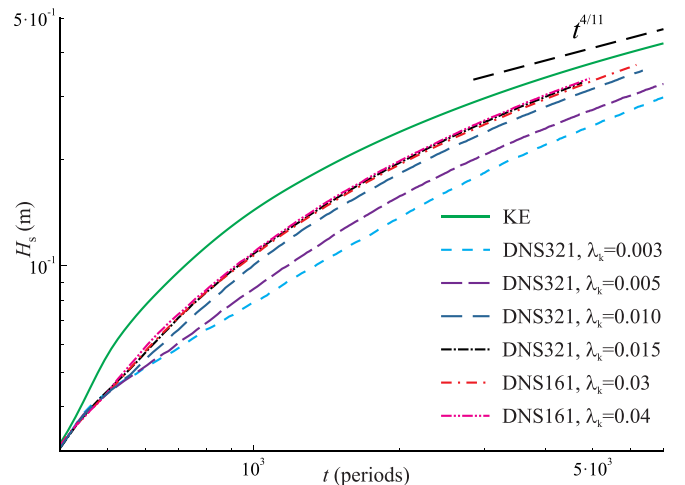
FIG. 4. Evolution of significant wave height H_s: DNS on 161×71 and 321×71 grids for different values of λ_k vs the KE simulation.

is relatively small and appears to be due to breaking that effectively reduces the forcing. Simulation of the KE with wind forcing reduced by 5% makes the difference insignificant.

Discussion. Studies of wave kinetics based on the KE rely on the homogeneity of the right-hand side of the equation with respect to the spectrum. This property is an artifact of the neglect of non-Gaussianity effects. In this Letter, we show that although non-Gaussianity is weak, in the long term it leads to a considerable discrepancy in the spectral shape. At the same time, the integral parameters of a wave field appear to be much less affected, with the error remaining within the uncertainty introduced by wave breaking, which the DNS modeling has to take into account. The spectral shape obtained by the DNS appears to be in much closer agreement with observations of mature sea states than the KE spectral shape.

The present study and its findings have numerous important implications. First, they are of crucial importance for all applications where the shape of the wave spectrum is significant, rather than just its integrated description, in particular for probability estimates of extreme wave events, design or coastal hazard risk assessments, sediment transport models, etc. Second, it is well known that the wind wave models based on the KE are optimized for certain frequency and directional resolutions against the available measurements. The knowledge of systematic errors in the models can drastically improve the quality of such optimizations, and thus improve the quality of wind wave modeling. Third, the findings of this Letter provide insight on the role of non-Gaussianity in kinetic models, which is significant for a wide context of wave turbulence in various branches of physics.

[1] V. Zakharov, V. L'vov, and G. Falkovich, *Kolmogorov Spectra of Turbulence I: Wave Turbulence* (Springer, Berlin, 1992), p. 264.

[2] A. C. Newell and B. Rumpf, in *Advances in Wave Turbulence*, edited by V. Shrira and S. Nazarenko, Vol. 83 of World Scientific Series on Nonlinear Science Series A (World Scientific, Singapore, 2013), pp. 1–51.

[3] K. Hasselmann, J. Fluid Mech. **12**, 481 (1962).

[4] G. Komen, L. Cavaleri, M. Donelan, K. Hasselmann, S. Hasselmann, and P. A. E. M. Janssen, *Dynamics and Modelling of Ocean Waves* (Cambridge University Press, Cambridge, UK, 1994), p. 532.

[5] Y. Toba, J. Oceanogr. Soc. Jpn. **28**, 109 (1972).

[6] K. Hasselmann, D. Ross, P. Muller, and W. Sell, J. Phys. Oceanogr. **6**, 200 (1976).

[7] D. Resio, L. Vincent, and D. Ardag, Ocean Modell. **103**, 38 (2016).

[8] V. Zakharov, S. Badulin, P. Hwang, and G. Caulliez, J. Fluid Mech. **780**, 503 (2015).

[9] S. Badulin, A. Pushkarev, D. Resio, and V. Zakharov, Nonlin. Process. Geophys. **12**, 891 (2005).

[10] L. Holthuijsen, *Waves in Oceanic and Coastal Waters* (Cambridge University Press, Cambridge, UK, 2007), p. 404.

[11] A. Babanin and Y. Soloviev, J. Phys. Oceanogr. **28**, 563 (1998).

[12] C. E. Long and D. T. Resio, J. Geophys. Res. **112**, C05001 (2007).

[13] L. Romero and W. Melville, J. Phys. Oceanogr. **40**, 466 (2010).

[14] W. J. Pierson, Jr. and L. Moskowitz, J. Geophys. Res. **69**, 5181 (1964).

[15] J. Alves, M. Banner, and I. Young, J. Phys. Oceanogr. **33**, 1301 (2003).

[16] M. Banner, A. Babanin, and I. Young, J. Phys. Oceanogr. **30**, 3145 (2000).

[17] S. Annenkov and V. Shrira, J. Fluid Mech. **561**, 181 (2006).

[18] S. Annenkov and V. Shrira, J. Fluid Mech. **726**, 517 (2013).

[19] V. Shrira and S. Annenkov, in *Advances in Wave Turbulence* (Ref. [2]), Chap. 7, pp. 239–281.

[20] S. Annenkov and V. Shrira, J. Fluid Mech. **844**, 766 (2018).

[21] V. Zakharov, Eur. J. Mech. B Fluids **18**, 327 (1999).

[22] M. Onorato and G. Dematteis, J. Phys. Commun. **4**, 095016 (2020).

[23] A. Newell, S. Nazarenko, and L. Biven, Physica D **152-153**, 520 (2001).

[24] S. Hsiao and O. Shemdin, J. Geophys. Res. **88**, 9841 (1983).

[25] See Supplemental Material at http://link.aps.org/supplemental/10.1103/PhysRevE.106.L042102 for a detailed discussion of the DNS algorithm and the choice of parameters, which includes Refs. [26–30].

[26] V. E. Zakharov, J. Appl. Mech. Tech. Phys. **9**, 190 (1968).

[27] K. Trulsen and K. Dysthe, Wave Motion **24**, 281 (1996).

[28] S. Annenkov and V. Shrira, J. Fluid Mech. **449**, 341 (2001).

[29] S. Y. Annenkov and V. I. Shrira, Phys. Rev. Lett. **102**, 024502 (2009).

[30] S. Y. Annenkov and V. I. Shrira, Phys. Rev. Lett. **107**, 114502 (2011).